
This is an electronic reprint of the original article.
This reprint may differ from the original in pagination and typographic detail.

Conley, Kevin; Karttunen, Antti J.

Overcoming the Sticking Point: Electrical Conductivity of Carbon Nanotube Networks Containing 3d Metals

Published in:
Journal of Physical Chemistry C

DOI:
[10.1021/acs.jpcc.2c08770](https://doi.org/10.1021/acs.jpcc.2c08770)

Published: 04/05/2023

Document Version
Publisher's PDF, also known as Version of record

Published under the following license:
CC BY

Please cite the original version:
Conley, K., & Karttunen, A. J. (2023). Overcoming the Sticking Point: Electrical Conductivity of Carbon Nanotube Networks Containing 3d Metals. *Journal of Physical Chemistry C*, 127(17), 8208–8216.
<https://doi.org/10.1021/acs.jpcc.2c08770>

This material is protected by copyright and other intellectual property rights, and duplication or sale of all or part of any of the repository collections is not permitted, except that material may be duplicated by you for your research use or educational purposes in electronic or print form. You must obtain permission for any other use. Electronic or print copies may not be offered, whether for sale or otherwise to anyone who is not an authorised user.

Overcoming the Sticking Point: Electrical Conductivity of Carbon Nanotube Networks Containing 3d Metals

Kevin Conley* and Antti J. Karttunen*



Cite This: *J. Phys. Chem. C* 2023, 127, 8208–8216



Read Online

ACCESS |



Metrics & More

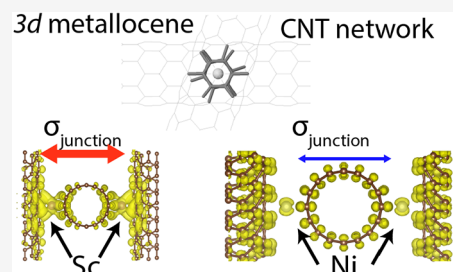


Article Recommendations



Supporting Information

ABSTRACT: Carbon nanotubes have excellent electrical conductivity along the length of the tubes. Yet, the electrical conductivity across the nanotube–nanotube intersections is weak and severely limits device performance. Here, we show that the incorporation of 3d metal (period 4) atoms into networks of semiconducting (8,0) carbon nanotubes significantly enhances the electrical conductivity within the network. Our calculations using quantum mechanical methods and semiclassical Boltzmann transport theory predict the changes to the electronic structure and provide directional information about the flow of electrons within the network. The ligand field splitting of the transition metals exerts strong effects on the conductivity. Interestingly, networks doped with Sc, V, or Fe can become insulating along certain directions or have higher conductivity across the junction than along the tubes. This finding suggests that doping with transition metals removes a bottleneck of charge transport within carbon nanotube films.



INTRODUCTION

Metallocenes are a class of organometallic compounds consisting of a metal atom coordinated between cyclic aromatics.^{1–3} Transition metal atoms sandwiched between the aromatic rings form haptic, covalent bonds. The versatile d electron configuration strongly interacts with the delocalized π -electron system and leads to organometallic complexes with adaptable catalytic or optoelectronic properties.^{2,4} The integration of metallocenes into polymer networks^{5,6} or multiple-decker structures^{7–9} broadens their applications to materials science areas, such as energy conversion and storage, optics, and electrical conductivity.

Carbon nanotubes (CNTs) are model platforms to explore the organometallic coordination and interaction of extended π -electrons with dopants. Immobilized or thin films of CNTs are signal amplifiers in biosensors,¹⁰ chemical sensors, and touch screen devices.^{11–16} The electrical conductivity within thin films is affected by the CNT chirality and network morphology.^{16–19} Localized atomic force microscopy experiments demonstrate that the charge transport across the CNT crossing regions (i.e., intersections) are a limiting step.^{20–22} Computational methods, such as standard percolation theory and charge carrier transport models, consider morphological effects in predicting the electrical transport through a network but lack detailed electronic structure information.^{16–19}

Previous studies investigated the electronic structure of CNTs containing analytes or dopants using density functional theory (DFT) methods. Intense Raman peaks have been observed from nanotubes with encapsulated S.²³ The adsorption of H₂ was more favorable on transition-metal-decorated CNTs than pristine CNTs.^{24–26} NO₃, AuCl₃, AuCl₄, or halogens induce p-type behavior in semiconducting CNT networks.^{27–30} Atomic

gold clusters at the CNT intersection increase the electrical conductivity if the clusters have an odd number of atoms.³¹

Transition metal doping is an avenue to access organometallic properties in CNT films. Previously, Cr, Mo, and W were shown to form bis-hexahapto bonding at carbon nanotube intersections [$(\eta^6\text{-CNT})_2\text{M}$] and reduce the electrical resistance across the intersection.^{32–36} Improved conductivity and sheet resistance were also observed experimentally in films containing 3d metals (Ti, V, Mn, and Fe).^{37,38} The experimental findings were supported by calculations based on Green's function methods that show an improved charge transport through the junction of intersecting nanotubes doped with group 6 transition metal atoms.^{39,40} In a computational study using Landauer formalism, the quantum conductance across two parallel CNT ends is vastly enhanced when the nanotubes are bridged by a metallocene linker atom (Sc, Ti, V, Cr, Co, or Ni).⁴¹ However, the calculations only extract the quantum conductance parallel to the nanotubes. Comprehensive DFT computational studies of the directional electrical conductivity of CNT networks doped with transition metal atoms are lacking.

Recently, the electrical conductivity of CNT networks containing Group 11 or s–p metal dopants were calculated using DFT methods and semiclassical Boltzmann transport theory.⁴² The three-dimensional periodicity enabled the

Received: December 15, 2022

Revised: March 2, 2023

Published: April 20, 2023



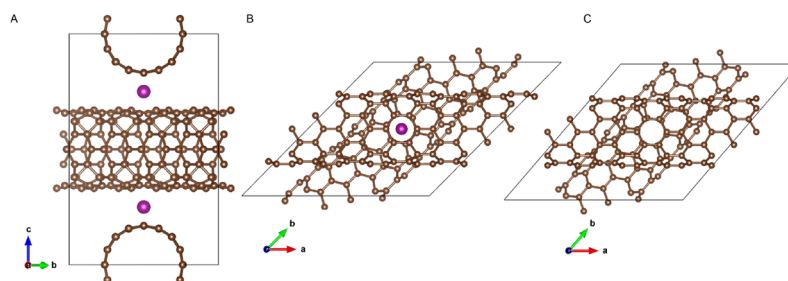


Figure 1. Network of (8,0) carbon nanotubes either (a,b) doped with transition metal atoms or (c) pristine, as viewed from the side or top-down. The doped networks have one transition metal atom per nanotube. The carbon atoms are brown, and the transition metal atoms (Mn) are purple. The networks belong to the *Cccm* (66) centrosymmetric space group.

electrical conductivity to be calculated both along the nanotubes and across the intersection. The dopants strengthen the conductivity in all directions and remove the bottleneck of charge transport within networks of mixed chiralities.

Here, we investigate carbon nanotube networks doped with 3d metals, K, or Ca using DFT and semiclassical Boltzmann transport theory. The focus is on homogeneous networks of (8,0) semiconducting nanotubes. Charge transport within CNT thin films with heterogeneous chirality is expected to be limited by the semiconducting tubes. First, the geometry of carbon nanotube networks containing 3d metal atoms are analyzed. Then, the effects of the dopants on the electronic structure and its influence on the electrical conductivity along the nanotubes and across the intersections are examined.

METHODS

All calculations presented in this work are performed with CRYSTAL17.⁴³ Networks of (8,0) carbon nanotubes were constructed with periodicity in three dimensions. The nanotubes lie along \vec{a} and \vec{b} , and $\alpha = \beta = 90^\circ$. The CNT intersection angle is equivalent to γ . Semiconducting nanotubes with (8,0) chirality are examined because of the limiting effect of semiconducting nanotubes on charge transport within networks.⁴² Transition metal atoms adopt metallocene-like coordination with carbon nanotubes.^{32–38} Therefore, two 3d metal atoms were situated between the nanotubes at the intersection (Figure 1). The atomic positions and lattice constants of the pristine and doped networks were relaxed to their minimum energy geometric conformation. During preliminary calculations on a doped network containing Ti atoms without any symmetry constraints (space group *P1*), the optimization ended up in a minimum geometry in space group *Cccm* (66). Thereafter, all pristine and doped networks were optimized in the centrosymmetric space group *Cccm*. The consistent space group of all networks enabled systematic comparison of the qualitative trends of the metallocene-like coordination across the period. One dopant atom per nanotube occupies both junctions and is necessary to examine the behavior of networks with periodicity in three dimensions. Other concentrations were not considered. The networks are overall neutral.

We applied the PBE0 hybrid density functional method with 25% Hartree–Fock and 75% PBE exchange^{44,45} and utilized Gaussian-type basis sets based on the molecular Karlsruhe basis sets.⁴⁶ Triple- ζ -valence + polarization (TZVP) level basis sets were used for C⁴⁷ and 3d metals.⁴⁸ Split-valence + polarization (SVP) level basis sets were used for K⁴⁹ and Ca.⁴² Spin polarization was taken into account in all networks because of the open-shell nature of some of the dopants. The reciprocal

space was sampled using a Monkhorst–Pack-type $2 \times 2 \times 2$ *k*-point mesh. The calculations were carried out with Coulomb and exchange integral tolerance factors (TOLINTEG) set to tight values of 8, 8, 8, 8, and 16.

The main aim was to characterize the qualitative trends in electrical conductivity resulting from doped CNT networks. Thus, the trends were investigated without van der Waals effects, and the conductivity was analyzed relative to the pristine network. The electrical conductivity, σ , at temperature, T , equal to 300 K was obtained using Boltzmann transport theory, as implemented in CRYSTAL17.⁵⁰ The transport coefficient was solved within the constant relaxation time and rigid band approximations, such that

$$[\sigma]_{qr}(\mu, T) = e^2 \int dE \left(-\frac{\partial f_0(\mu, T)}{\partial E} \right) \Xi_{qr}(E) \quad (1)$$

where the energy is E ; the Fermi–Dirac distribution is f_0 ; the Fermi level is μ ; and the transport coefficients, $\Xi_{qr}(E)$, are defined as

$$\Xi_{qr}(E) = \tau \sum_{\mathbf{k}} \frac{1}{N_{\mathbf{k}}} \frac{1}{V} \sum_{i,j} v_{i,q}(\mathbf{k}) v_{j,r}(\mathbf{k}) \delta(E - E_i(\mathbf{k})) \quad (2)$$

$v_{i,q}$ was the velocity of the i^{th} band along q ; $N_{\mathbf{k}}$ is the number of *k*-points over the cell volume, V ; and the lifetime, τ , was 1 fs for all studied systems. The conductivity is shown as the summation of the α and β spin states. The in-plane conductivity and junction conductivities at the Fermi level are reported for the doped networks relative to the pristine network. The relative in-plane conductivity (σ_{plane}^*) is the average along the x and y axes, and the junction conductivity (σ_{junc}^*) is along z , i.e., across the junction.

The reciprocal space paths for the electronic band structures were obtained from the SeeK-path service⁵¹ (see Figure S1 for reciprocal space and Brillouin-zone information). The density of states and electrical conductivities were obtained with a dense *k*-point mesh of $16 \times 16 \times 16$ and $8 \times 8 \times 8$, respectively.

RESULTS AND DISCUSSION

Network Geometry. The primitive cell lattice constants of the minimum energy geometries of the pristine and doped carbon nanotube networks are shown in Table 1. Interestingly, the transition metal can shrink the cell volume and the length of the unit cell across the junction, c . The contraction occurs because the transition metal atoms are situated between the nanotubes in a bis-hexahapto (η^6) metallocene-like coordination in the *Cccm* (66) centrosymmetric space group (Figure 2). The nanotubes are relaxed, and the CNT intersection angle, γ , is free to rotate during the optimization. The carbon atoms across

Table 1. Lattice Constant across Junction (c), Dopant-C Inter-Atomic Distance (M-C), CNT Intersection Angle (γ), and Cell Volume (V) of Pristine and Doped (8,0) CNT Networks

	c (Å)	M-C _a (Å)	M-C _b (Å)	M-C _c (Å)	γ (deg)	V (Å ³)
pristine	19.1				49.3	4165
K	23.6	3.01	3.24	3.24	65.1	6141
Ca	21.7	2.54	2.78	2.78	80.1	6138
Sc	20.7	2.30	2.57	2.57	72.0	5654
Ti	19.7	2.16	2.40	2.41	47.5	4182
V	19.6	2.13	2.37	2.37	54.4	4571
Cr	19.0	2.07	2.29	2.29	45.4	3880
Mn	18.6	2.07	2.26	2.26	45.3	3802
Fe	19.8	2.20	2.43	2.44	33.9	3172
Co	19.2	2.10	2.35	2.36	34.0	3085
Ni	20.0	2.25	2.48	2.48	33.8	3190
Cu	20.6	2.34	2.59	2.59	59.9	5109
Zn	24.0	3.14	3.38	3.38	67.8	6392

the junction are eclipsed when γ equals 60° and staggered when γ equals $60 \pm 30^\circ$. Networks doped with midperiod transition metals (Fe, Co, and Ni) have a more closely bound networks in a nearly staggered conformation. Furthermore, the distance c reflects the competition between the ionic radii⁵² and electronegativity⁵³ of the doping element across the periodic row. The larger, more diffuse atoms, such as Sc, form relatively long bonds with the carbon nanotubes. The more compact atoms are generally more electronegative and less willing to donate electrons. Consequently, the competition leads to a minimum value of c in the Mn-doped network. The trends in c are consistent with the interatomic distance between the C atoms in the metallocene-like coordination (M-C_a, M-C_b, and M-C_c). Each C is 4-fold degenerate because of the space group symmetry. The unequal distances are due to the curvature of the nanotube. The interatomic distances are similar to that between Cr and the C atoms in bis(η^6 -benzene) chromium (2.13 Å) calculated with the same exchange-correlation functional.

The binding energy and local environment of each dopant are summarized in Table 2. The partial Mulliken charge of each dopant (Z_M) is obtained by subtracting its Mulliken population from its atomic number (Z). As expected, electron density is shifted toward the carbon nanotube network, which results in a slightly positive dopant. s-p metals and Zn dopants have small Mulliken bond overlap populations between the metals and the nearest C atom (P_{MC}), thereby indicating ionic (K, Ca) or weak (Zn) interactions. The bond overlap populations of other 3d metals are rather similar. Covalent bonds form between the transition metal atoms and the carbon nanotube networks. The

Table 2. Binding Energy per Dopant, Mulliken Partial Charge of the Dopant (Z_M), and Mulliken Bond Overlap Population between the Dopant and the Nearest C Atom (P_{MC}) in (8,0) CNT Networks

	binding energy (kJ/mol)	Z_M	P_{MC}
K	-460	0.85	0.01
Ca	-700	1.38	0.03
Sc	-587	1.32	0.06
Ti	-706	1.19	0.05
V	-323	0.84	0.07
Cr	-102	0.68	0.06
Mn	23	0.52	0.07
Fe	-268	0.69	0.08
Co	-505	0.48	0.08
Ni	-507	0.57	0.07
Cu	-133	0.50	0.06
Zn	-27	0.08	0.02

binding energy of Mn is positive, which indicates the interaction is energetically unfavorable. Other 3d dopant atoms bind favorably to the network, and the binding energies range from -102 to -706 kJ/mol. There is a discontinuous decline across the period. The binding becomes generally less favorable from Ca to Mn and from Co to Zn. Cr, despite being known to form stable (bis)-hapto structures with polycyclic aromatics, has a relatively weak binding energy. This may be due to the stability of atomic Cr in the half-filled $4s^1 3d^5$ electron configuration. The Mn atom also has an energetically stable electron configuration ($4s^2 3d^5$), and networks containing Mn are less favorable. Similar binding energies were observed elsewhere.⁴¹ Zn is weakly bound to the network because of its fully filled d shell. The atom is not covalently bound to the nanotubes, and the network has the largest cell volume and c . We note that the binding energies of K, Ca, and Cu in these networks are different from those reported in our previous work⁴² because of the different space group symmetry.

Electronic Structure and Conductivity of the Doped Networks. Covalent bonds are formed between the carbon nanotubes and the transition metal atoms in the metallocene-like coordination. The 3d orbitals of the transition metal dopants are energetically positioned to strongly interact with the delocalized π -electron system of the (8,0) nanotube. The number of electrons and ligand field splitting during the bis-hapto bond formation lead to changes in the electronic properties of the networks.

In the pristine network, the electrical conductivity is weaker across the intersection than along the tubes, which is in agreement with previous work that did not enforce symme-

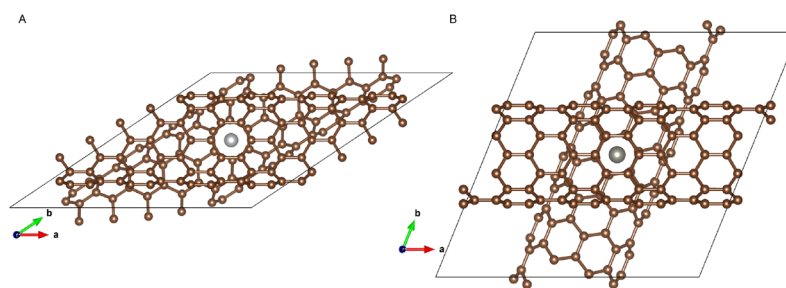


Figure 2. (8,0) CNT network doped with (a) Ni in a staggered conformation and (b) Zn in the eclipsed conformation. The CNT intersection angle, γ , is 33.8° and 67.8° , respectively. There is one dopant atom per nanotube.

try.^{39,42,54–56} This implies that the flow of electrons across the junction are a bottleneck of charge transport in pristine networks. The inclusion of transition metals can cause the semiconducting networks to become n-type or induce a gap state. A summary of the electronic properties and electrical conductivities of networks containing dopants along the 3d period are shown in Table 3. The electrical conductivities at the

Table 3. Electrical Conductivity of Pristine and Doped (8,0) CNT Networks at the Fermi Level Reported Relative to the Pristine (8,0) Network Intersecting at 49° (2 S/m across the Junction and 9477 S/m in the Plane of the Tubes)

	gap ^a (eV)	spin	σ_{plane}^*	σ_{junc}^*
pristine	1.49	0.0	1.0	1.0
K	n-type	0.0	8.4	0.0
Ca	n-type	0.0	1.3	2505.5
Sc	gap state	0.0	0.5	4166.0
Ti	0.98	0.0	0.2	76.0
V	gap state	0.0	0.1	2701.5
Cr	1.08	0.0	0.3	45.0
Mn	n-type	0.0	8.2	545.0
Fe	half-filled metal	4.0	0.0	304.0
Co	n-type	0.0	0.7	4256.0
Ni	n-type	2.2	5.6	8.0
Cu	n-type	0.0	7.4	21.0
Zn	1.21	0.0	0.0	122.0

^a“n-Type” means that the pseudogap lies below the Fermi level, and “gap state” means that the Fermi level lies at a state in the pseudogap.

Fermi level across the junction and in the plane of the nanotubes are reported relative to the pristine network. Notably, the charge transport across the junction is enhanced in all dopants

considered except K. Transition metal linker atoms (Sc, Ti, V, Cr, Co, or Ni) were previously shown to enhance the electrical transport along two parallel CNTs.⁴¹ The current results show that the improvement is several orders of magnitude greater across the intersection than along the tubes.

The relative conductivity increases along the nanotubes of all the n-type networks except the one containing Co. The shift of the Fermi level into the conduction band enhances the charge transfer. Of the networks doped with transition metals, Mn improves the conductivity along the nanotubes the most (8.2-fold). The network containing Co is unique because of the d character and discrete order at the conduction band edge. Similar improvements were previously reported in n-type networks containing other dopants including Group 11 and s–p metals (K, Ca, and Al).⁴² By contrast, the relative electrical conductivity along the tubes worsens in all doped networks with a band gap or gap state. These networks cannot overcome the localization of the extended π -electron system by the 3d states, thereby reducing the electron flow.

The dopant facilitates charge transport across the junction. The 3d π orbital mixing localizes the electron density at the intersection bridging the nanotubes. The bridging is confirmed by visualizing the band-projected charge density. For example, in the Sc-doped network, the charge density of band 789 extends over the transition metal and across the junction (Figure 3). This network had the second largest relative conductivity across the junction (4166-fold). Furthermore, the charge density extends evenly along the tubes, which suggests the charge transfer is not preferential on a particular tube. By comparison, the pristine carbon nanotube network has no bridging.

The enhanced electrical conductivity of the doped networks is also apparent in the band velocity near the Fermi level (Figure

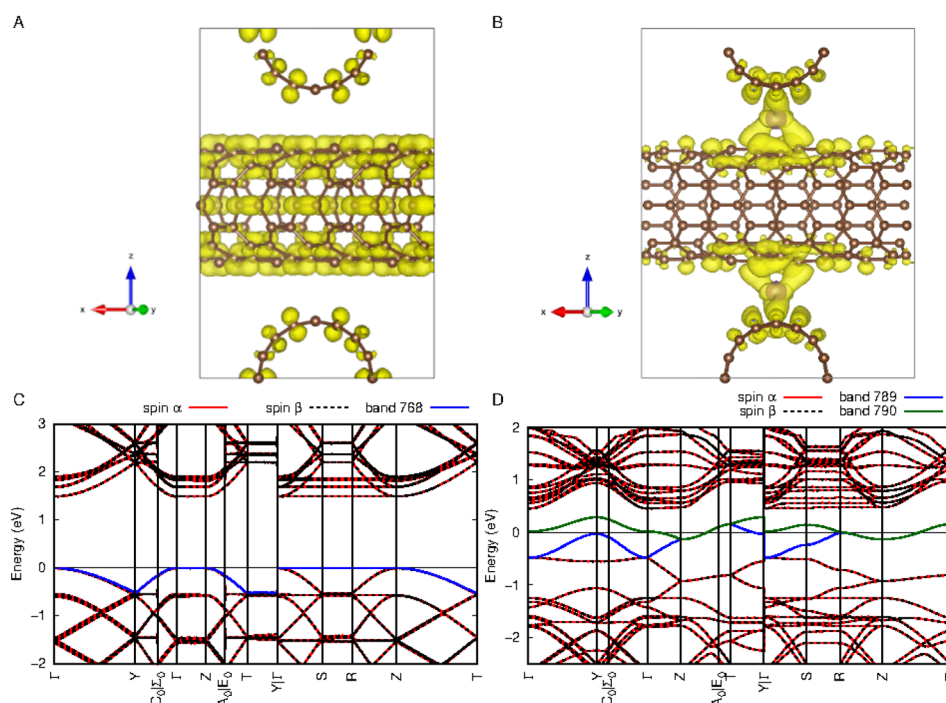


Figure 3. Projected charge density of the topmost band of the (a) pristine (band 768) and (b) Sc-doped (band 789) (8,0) CNT network. The isovalue is $4 \times 10^{-4} e/a_0^3$. The band occupancy is 2.0 electrons in the pristine networks and 1.5 electrons in the doped network ($\alpha + \beta = 1.5$ and $\alpha - \beta = 0.0$). The band structures of the (c) pristine and (d) Sc-doped networks. The energy is reported relative to the Fermi level, and there is one dopant atom per nanotube.

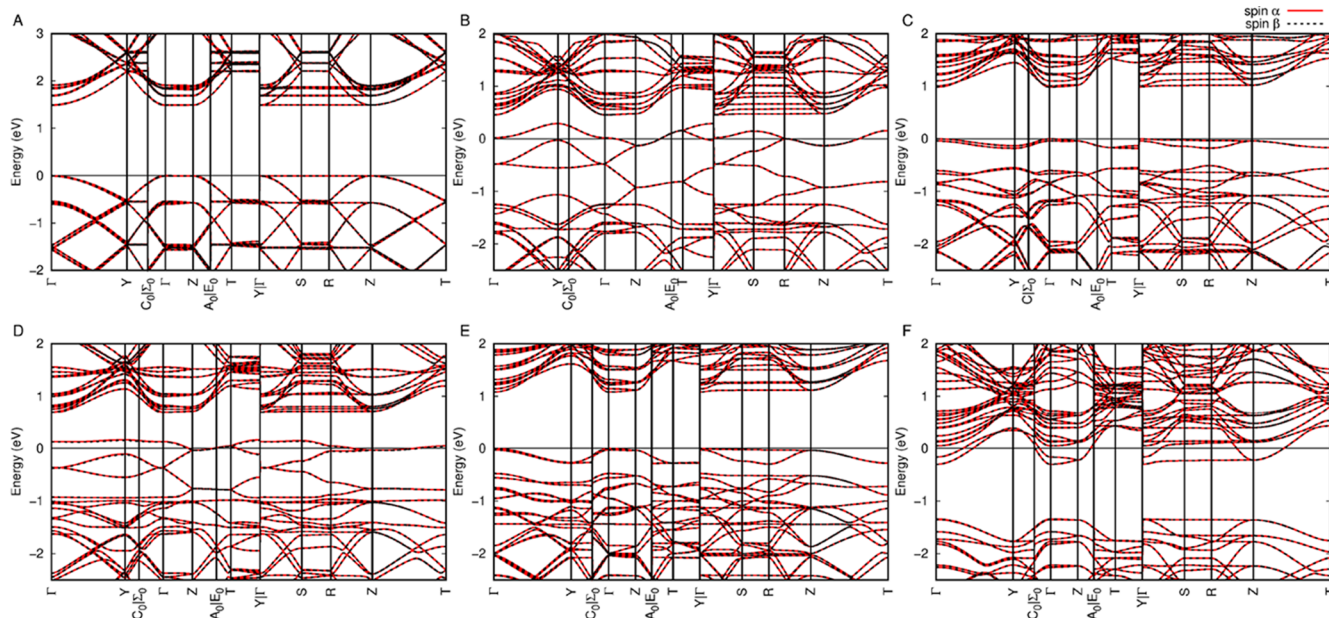


Figure 4. Bands of (a) pristine and (8,0) CNT networks doped with (b) Sc, (c) Ti, (d) V, (e) Cr, and (f) Mn. There is one dopant atom per nanotube. The energy is reported relative to the Fermi level. The band gap of the pristine network is 1.49 eV, and the network doped with Mn is n-type. The networks doped with Sc or V have a gap state, and the networks doped with Ti or Cr have a band gap of 0.98 and 1.08 eV, respectively.

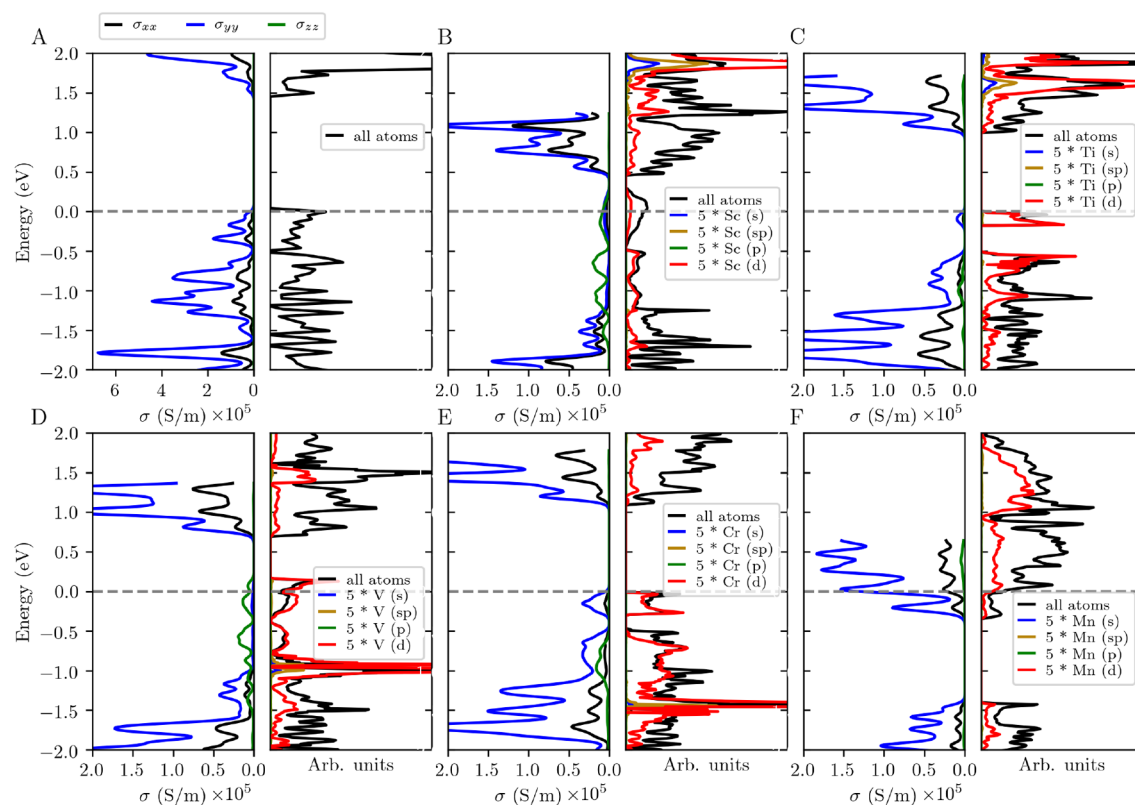


Figure 5. Electrical conductivity and density of states of (a) pristine (with symmetry imposed, 49° intersection angle) and (8,0) CNT networks doped with (b) Sc, (c) Ti, (d) V, (e) Cr, and (f) Mn. There is one dopant atom per nanotube. The energies are reported with respect to the Fermi level.

3). The band dispersion across the junction (Γ – Z) is significantly larger in the doped network than the pristine networks. The Sc-doped network is metallic, and its overlapping midgap states (bands 789 and 790) have an occupancy of 1.5 and 0.5, respectively. By contrast, the bands in the pristine

network are highly dispersive along Γ – Y and Γ – S (in the plane of the nanotube axes) but not along Γ – Z (across the junction).

The variation in the properties of different transition metal dopants is in part explained by the number of d electrons. It is most noticeable in networks containing early period transition metals where the ligand field splitting is similar and near the

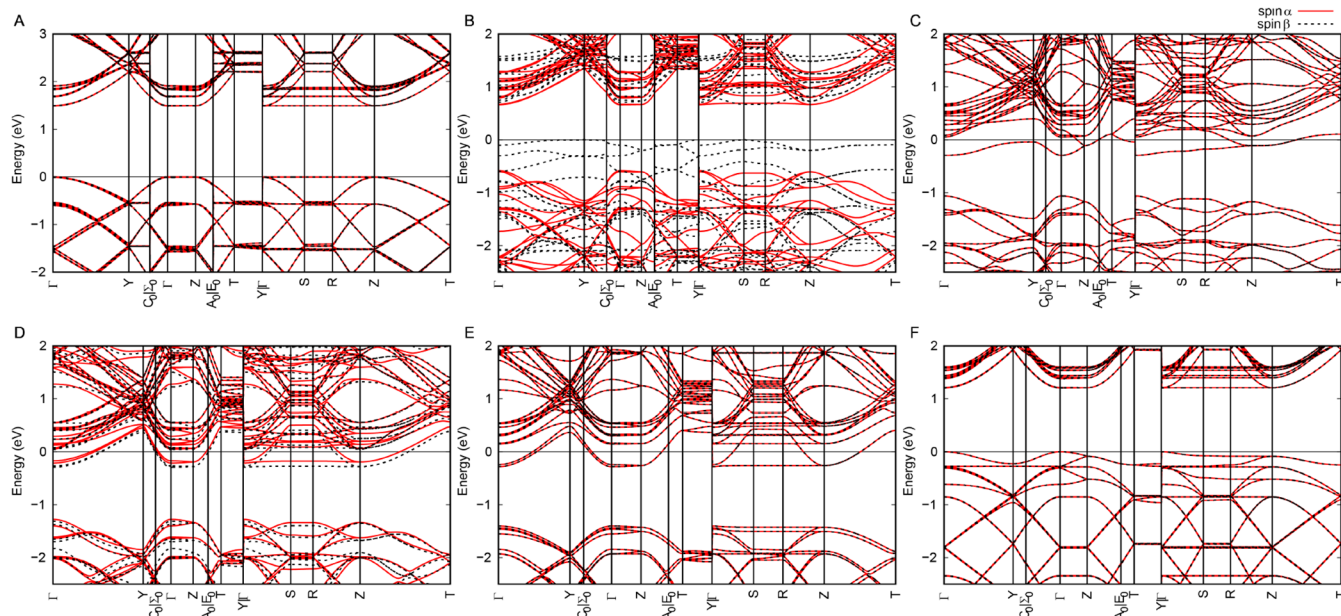


Figure 6. Bands of (a) pristine and (8,0) CNT networks doped with (b) Fe, (c) Co, (d) Ni, (e) Cu, and (f) Zn. There is one dopant atom per nanotube. The energy is reported relative to the Fermi level. The band gap of the pristine network is 1.49 eV, and the network doped with Fe is a half-filled metal. The networks doped with Co, Ni, or Cu are n-type, and the network doped with Zn has a band gap of 1.21 eV.

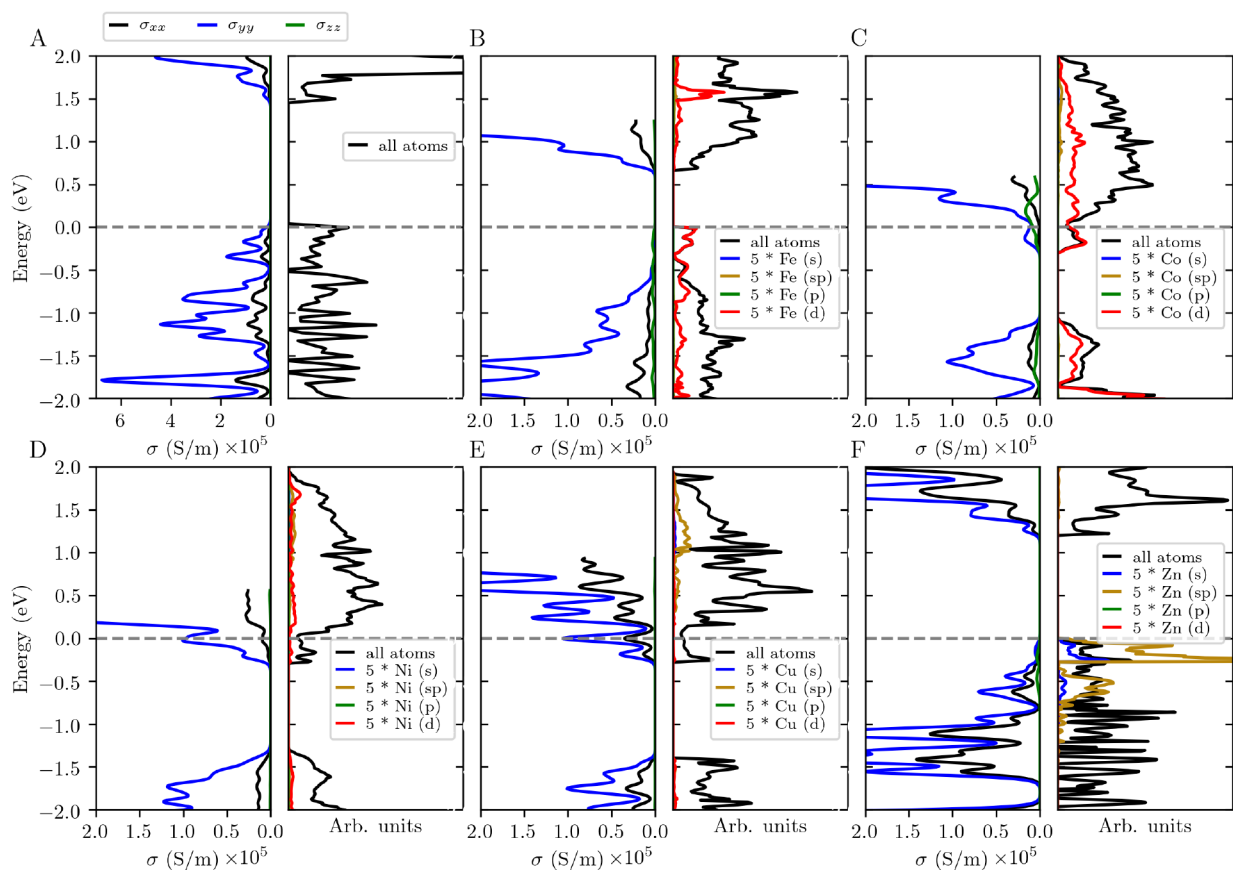


Figure 7. Electrical conductivity and density of states of (a) pristine (with symmetry imposed, 49° intersection angle) and (8,0) CNT networks doped with (b) Fe, (c) Co, (d) Ni, (e) Cu, and (f) Zn. There is one dopant atom per nanotube.

Fermi level. The band structures are shown in Figure 4. Additional d electrons raise the Fermi level and change the network type. For example, the metallic network containing Sc

becomes semiconducting when the dopant is changed to Ti. This occurs because the additional electrons occupy the midgap states. There is a similar progression between V and Cr. Both Sc-

and V-doped networks are metallic with partially filled midgap states, and their band structures resemble each other. The degeneracy at the *R* special point in the network containing Sc is lifted in the V-doped network. This contributes to the slightly reduced conductivity compared with the Sc-doped network.

The conductivities along each nanotube and across the junction are seen in Figure 5. In stark contrast to pristine networks, the conductivity at the Fermi level is smaller along either nanotube than across the junction containing Sc or V. Explicit conductivities at the Fermi level are provided in Table S1. The doping alters the easiest direction of electron flow from along the tubes to across the junction. This suggests that it is possible for the bottleneck of charge transport to switch to along the nanotubes. The asymmetry of the electrical conductivity along the nanotubes is due to the rotation of the unit cell vectors from the Cartesian coordinate axis. This asymmetry occurs when the tubes intersect at angles other than 90° and has been discussed elsewhere.⁴²

Networks containing late period elements (Mn and beyond) or s–p metal dopants are n-type metallic networks, with the exceptions of Fe and Zn. The networks have bands with high velocity along the nanotube (Figure 6). The regular band structure of the pristine network is disrupted by the doping, which can increase dispersion across the junction. The Fe-doped network has a half-filled zone. Its total spin multiplicity is 4.0 (cf. Table 3). The high spin state is due to the worsening Fermi level alignment and weakening of the ligand field splitting. Across the period, the d states lower in energy, as seen in the orbital projected densities of states in Figures 5, 7, and S2. The top of the valence band of the network containing Zn has contributions from s and sp orbitals of the dopant because of its filled 3d subshell. High-spin states are typical in Fe organometallics.⁵⁷ Similar effects are seen in the network containing Ni, which has a total spin multiplicity of 2.2. We note that the relative conductivities of the networks containing K, Ca, or Cu are different from those reported in our previous work⁴² because of the different space group symmetry.

CONCLUSIONS

The incorporation of transition metal atoms into carbon nanotube networks changes its electronic structure and electrical conductivity. At the junction of two CNTs, 3d metal atoms bind favorably in a metallocene-like coordination. Organometallic networks are found by the covalent bonding between the d electrons with the delocalized π -electron system. The versatile d electron configuration across the period changes the electrical transport of networks of semiconducting (8,0) carbon nanotubes.

The electrical transport of networks is enhanced when CNTs are linked by transition metal metallocenes.^{32–41} This work reveals the anisotropic effects of the electrical conductivity in different directions within the network using quantum mechanical methods and semiclassical Boltzmann transport theory. The largest improvement occurs across intersections bridged by a transition metal atom. The localization of electron density across the junction enhances the charge transport in all networks containing transition metals. Interestingly, dopants can enhance the intertube conductivity or suppress the conductivity along the tube to change the bottleneck of electrical conductivity within networks. Because of the changes to the adjacent sp² C atoms and delocalized π -system, the conductivity along the nanotubes remained large only for the n-type networks except the one containing Co. The conductivity

along the nanotubes can even become insulating when the networks contain Fe or Zn. This offers a possibility to form CNT thin films with adaptable catalytic or optoelectronic properties. Although concentration and local geometries would affect the performance of films, this work examines the trends of 3d metals in a bis-hexahapto (η^6) metallocene-like coordination. Quantification of the changes in different directions could improve models of network conductivity that lack a detailed electronic structure, such as percolation methods.

ASSOCIATED CONTENT

Supporting Information

The Supporting Information is available free of charge at <https://pubs.acs.org/doi/10.1021/acs.jpcc.2c08770>.

Information on the *k*-path and supplemental results of the directional conductivity of (8,0) networks (PDF)

Optimized structures in CIF format (ZIP)

AUTHOR INFORMATION

Corresponding Authors

Kevin Conley – Department of Chemistry and Materials Science, Aalto University School of Chemical Engineering, FI-00076 Aalto, Finland; orcid.org/0000-0001-7780-3096; Email: kevin.conley@aalto.fi

Antti J. Karttunen – Department of Chemistry and Materials Science, Aalto University School of Chemical Engineering, FI-00076 Aalto, Finland; orcid.org/0000-0003-4187-5447; Email: antti.karttunen@aalto.fi

Complete contact information is available at: <https://pubs.acs.org/doi/10.1021/acs.jpcc.2c08770>

Notes

The authors declare no competing financial interest.

ACKNOWLEDGMENTS

We acknowledge Business Finland for funding (Grant No. 3767/31/2019) and Finnish IT Center for Science (CSC) for computational resources.

REFERENCES

- (1) Seyferth, D. Bis(benzene)chromium. 2. Its discovery by EO Fischer and W. Hafner and subsequent work by the research groups of EO Fischer, HH Zeiss, F. Hein, C. Elschenbroich, and others. *Organometallics* **2002**, *21*, 2800–2820.
- (2) Pampaloni, G. Aromatic hydrocarbons as ligands. Recent advances in the synthesis, the reactivity and the applications of bis (η^6 -arene) complexes. *Coord. Chem. Rev.* **2010**, *254*, 402–419.
- (3) Astruc, D. Why is ferrocene so exceptional? *Eur. J. Inorg. Chem.* **2017**, *2017*, 6–29.
- (4) Braunschweig, H.; Damme, A.; Dück, K.; Krummenacher, I.; Paprocki, V.; Radacki, K.; Ramler, J.; Schiller, C.; Schneider, C. Boryl- and Silyl-Substituted Mixed Sandwich Compounds of Scandium. *Chem. Eur. J.* **2018**, *24*, 2403–2409.
- (5) Zhong, H.; Wang, G.; Song, Z.; Li, X.; Tang, H.; Zhou, Y.; Zhan, H. Organometallic polymer material for energy storage. *Chem. Commun.* **2014**, *50*, 6768–6770.
- (6) Liu, X.; Rapakousiou, A.; Deraedt, C.; Ciganda, R.; Wang, Y.; Ruiz, J.; Gu, H.; Astruc, D. Multiple applications of polymers containing electron-reservoir metal-sandwich complexes. *Chem. Commun.* **2020**, *56*, 11374–11385.
- (7) Yasuike, T.; Nakajima, A.; Yabushita, S.; Kaya, K. Why do vanadium atoms form multiple-decker sandwich clusters with benzene molecules efficiently? *J. Phys. Chem. A* **1997**, *101*, 5360–5367.

- (8) Masubuchi, T.; Ohi, K.; Iwasa, T.; Nakajima, A. Experimental and theoretical studies on the electronic properties of vanadium-benzene sandwich cluster anions, $V_nBz_{n+1}^-$ ($n = 1-5$). *J. Chem. Phys.* **2012**, *137*, 224305.
- (9) Nakajima, A. Study on electronic properties of composite clusters toward nanoscale functional advanced materials. *Bull. Chem. Soc. Jpn.* **2013**, *86*, 414–437.
- (10) Han, S.; Liu, W.; Zheng, M.; Wang, R. Label-free and ultrasensitive electrochemical DNA biosensor based on urchinlike carbon nanotube-gold nanoparticle nanoclusters. *Anal. Chem.* **2020**, *92*, 4780–4787.
- (11) Thostenson, E. T.; Ren, Z.; Chou, T.-W. Advances in the science and technology of carbon nanotubes and their composites: A review. *Compos. Sci. Technol.* **2001**, *61*, 1899–1912.
- (12) Kong, J.; Chapline, M. G.; Dai, H. Functionalized carbon nanotubes for molecular hydrogen sensors. *Adv. Mater.* **2001**, *13*, 1384–1386.
- (13) Star, A.; Joshi, V.; Skarupo, S.; Thomas, D.; Gabriel, J.-C. P. Gas sensor array based on metal-decorated carbon nanotubes. *J. Phys. Chem. B* **2006**, *110*, 21014–21020.
- (14) Li, C.; Thostenson, E. T.; Chou, T.-W. Sensors and actuators based on carbon nanotubes and their composites: A review. *Compos. Sci. Technol.* **2008**, *68*, 1227–1249.
- (15) Ishihara, S.; O'Kelly, C. J.; Tanaka, T.; Kataura, H.; Labuta, J.; Shingaya, Y.; Nakayama, T.; Ohsawa, T.; Nakanishi, T.; Swager, T. M. Metallic versus semiconducting SWCNT chemiresistors: A case for separated SWCNTs wrapped by a metallocsupramolecular polymer. *ACS Appl. Mater. Interfaces* **2017**, *9*, 38062–38067.
- (16) Schroeder, V.; Savagatrup, S.; He, M.; Lin, S.; Swager, T. M. Carbon nanotube chemical sensors. *Chem. Rev.* **2019**, *119*, 599–663.
- (17) Buldum, A.; Lu, J. P. Contact resistance between carbon nanotubes. *Phys. Rev. B* **2001**, *63*, 161403.
- (18) Maarouf, A. A.; Mele, E. J. Low-energy coherent transport in metallic carbon nanotube junctions. *Phys. Rev. B* **2011**, *83*, 045402.
- (19) Zorn, N. F.; Zaumseil, J. Charge transport in semiconducting carbon nanotube networks. *Appl. Phys. Rev.* **2021**, *8*, 041318.
- (20) Stadermann, M.; Papadakis, S.; Falvo, M. R.; Novak, J.; Snow, E.; Fu, Q.; Liu, J.; Fridman, Y.; Boland, J.; Superfine, R.; et al. Nanoscale study of conduction through carbon nanotube networks. *Phys. Rev. B* **2004**, *69*, 201402.
- (21) Hu, L.; Hecht, D. S.; Gruner, G. Carbon nanotube thin films: fabrication, properties, and applications. *Chem. Rev.* **2010**, *110*, 5790–5844.
- (22) Znidarsic, A.; Kaskela, A.; Laiho, P.; Gaberscek, M.; Ohno, Y.; Nasibulin, A. G.; Kauppinen, E. I.; Hassanien, A. Spatially resolved transport properties of pristine and doped single-walled carbon nanotube networks. *J. Phys. Chem. C* **2013**, *117*, 13324–13330.
- (23) Li, G.; Fu, C.; Oviedo, M. B.; Chen, M.; Tian, X.; Bekyarova, E.; Itkis, M. E.; Wong, B. M.; Guo, J.; Haddon, R. C. Giant Raman response to the encapsulation of sulfur in narrow diameter single-walled carbon nanotubes. *J. Am. Chem. Soc.* **2016**, *138*, 40–43.
- (24) Du, A.; Smith, S. C. Van der Waals-corrected density functional theory: Benchmarking for hydrogen–nanotube and nanotube–nanotube interactions. *Nanotechnology* **2005**, *16*, 2118.
- (25) Dag, S.; Ozturk, Y.; Ciraci, S.; Yildirim, T. Adsorption and dissociation of hydrogen molecules on bare and functionalized carbon nanotubes. *Phys. Rev. B* **2005**, *72*, 155404.
- (26) Luna, C. R.; Verdinelli, V.; German, E.; Seitz, H.; Volpe, M. A.; Pistonesi, C.; Jasen, P. V. Hydrogen adsorption and associated electronic and magnetic properties of Rh-decorated (8, 0) carbon nanotubes using density functional theory. *J. Phys. Chem. C* **2015**, *119*, 13238–13247.
- (27) Murat, A.; Rungger, I.; Jin, C.; Sanvito, S.; Schwingschlögl, U. Origin of the p-type character of AuCl₃ functionalized carbon nanotubes. *J. Phys. Chem. C* **2014**, *118*, 3319–3323.
- (28) Ketolainen, T.; Havu, V.; Puska, M. Conductivity of AuCl₄-functionalized carbon nanotube networks. *J. Phys. Chem. C* **2017**, *121*, 4627–4634.
- (29) Janas, D.; Milowska, K. Z.; Bristowe, P. D.; Koziol, K. K. Improving the electrical properties of carbon nanotubes with interhalogen compounds. *Nanoscale* **2017**, *9*, 3212–3221.
- (30) Ketolainen, T.; Havu, V.; Jónsson, E.; Puska, M. Electronic transport properties of carbon-nanotube networks: The effect of nitrate doping on intratube and intertube conductances. *Phys. Rev. Appl.* **2018**, *9*, 034010.
- (31) Khoo, K. H.; Chelikowsky, J. R. Electron transport across carbon nanotube junctions decorated with Au nanoparticles: Density functional calculations. *Phys. Rev. B* **2009**, *79*, 205422.
- (32) Sarkar, S.; Niyogi, S.; Bekyarova, E.; Haddon, R. C. Organometallic chemistry of extended periodic π -electron systems: Hexahaptochromium complexes of graphene and single-walled carbon nanotubes. *Chem. Sci.* **2011**, *2*, 1326–1333.
- (33) Kalinina, I.; Bekyarova, E.; Sarkar, S.; Wang, F.; Itkis, M. E.; Tian, X.; Niyogi, S.; Jha, N.; Haddon, R. C. Hexahapto-Metal Complexes of Single-Walled Carbon Nanotubes. *Macromol. Chem. Phys.* **2012**, *213*, 1001–1019.
- (34) Tian, X.; Moser, M. L.; Pekker, A.; Sarkar, S.; Ramirez, J.; Bekyarova, E.; Itkis, M. E.; Haddon, R. C. Effect of atomic interconnects on percolation in single-walled carbon nanotube thin film networks. *Nano Lett.* **2014**, *14*, 3930–3937.
- (35) Pekker, A.; Chen, M.; Bekyarova, E.; Haddon, R. C. Photochemical generation of bis-hexahapto chromium interconnects between the graphene surfaces of single-walled carbon nanotubes. *Mater. Horiz.* **2015**, *2*, 81–85.
- (36) Chen, M.; Li, W.; Kumar, A.; Li, G.; Itkis, M. E.; Wong, B. M.; Bekyarova, E. Covalent atomic bridges enable unidirectional enhancement of electronic transport in aligned carbon nanotubes. *ACS Appl. Mater. Interfaces* **2019**, *11*, 19315–19323.
- (37) Wang, F.; Itkis, M. E.; Bekyarova, E.; Sarkar, S.; Tian, X.; Haddon, R. C. Solid-state Bis-hexahapto-metal complexation of single-walled carbon nanotubes. *J. Phys. Org. Chem.* **2012**, *25*, 607–610.
- (38) Wang, F.; Itkis, M. E.; Bekyarova, E. B.; Tian, X.; Sarkar, S.; Pekker, A.; Kalinina, I.; Moser, M. L.; Haddon, R. C. Effect of first row transition metals on the conductivity of semiconducting single-walled carbon nanotube networks. *Appl. Phys. Lett.* **2012**, *100*, 223111.
- (39) Ketolainen, T.; Havu, V.; Puska, M. J. Enhancing conductivity of metallic carbon nanotube networks by transition metal adsorption. *J. Chem. Phys.* **2015**, *142*, 054705.
- (40) Tan, J.; He, X.; Liu, X.; Zhao, M. Intrinsic current–voltage characteristics of metal-carbon nanotube networks: A first-principles study. *Org. Electron.* **2016**, *31*, 278–286.
- (41) Li, E. Y.; Marzari, N. Improving the electrical conductivity of carbon nanotube networks: A first-principles study. *ACS Nano* **2011**, *5*, 9726–9736.
- (42) Conley, K.; Karttunen, A. Bridging the junction: Electrical conductivity of carbon nanotube networks. *J. Phys. Chem. C* **2022**, *126*, 17266–17274.
- (43) Dovesi, R.; Erba, A.; Orlando, R.; Zicovich-Wilson, C. M.; Civalieri, B.; Maschio, L.; Rérat, M.; Casassa, S.; Baima, J.; Salustro, S.; et al. Quantum-mechanical condensed matter simulations with CRYSTAL. *WIREs Computational Molecular Science* **2018**, *8*, e1360.
- (44) Perdew, J. P.; Burke, K.; Ernzerhof, M. Generalized gradient approximation made simple. *Phys. Rev. Lett.* **1996**, *77*, 3865–3868.
- (45) Adamo, C.; Barone, V. Toward reliable density functional methods without adjustable parameters: The PBE0 model. *J. Chem. Phys.* **1999**, *110*, 6158–6170.
- (46) Weigend, F.; Ahlrichs, R. Balanced basis sets of split valence, triple zeta valence and quadruple zeta valence quality for H to Rn: Design and assessment of accuracy. *Phys. Chem. Chem. Phys.* **2005**, *7*, 3297–3305.
- (47) Karttunen, A. J.; Tynell, T.; Karppinen, M. Atomic-level structural and electronic properties of hybrid inorganic–organic ZnO: Hydroquinone superlattices fabricated by ALD/MLD. *J. Phys. Chem. C* **2015**, *119*, 13105–13114.
- (48) Kuklin, M. S.; Eklund, K.; Linnerna, J.; Ropponen, A.; Tolvanen, N.; Karttunen, A. J. Structural Properties and Magnetic Ground States

of 100 Binary *d*-Metal Oxides Studied by Hybrid Density Functional Methods. *Molecules* **2022**, *27*, 874.

(49) Stene, R. E.; Scheibe, B.; Karttunen, A. J.; Petry, W.; Kraus, F. Lewis Acidic Behavior of MoOF₄ towards the Alkali Metal Fluorides in Anhydrous Hydrogen Fluoride Solutions. *Eur. J. Inorg. Chem.* **2019**, *2019*, 3672–3682.

(50) Sansone, G.; Ferretti, A.; Maschio, L. Ab initio electronic transport and thermoelectric properties of solids from full and range-separated hybrid functionals. *J. Chem. Phys.* **2017**, *147*, 114101.

(51) Hinuma, Y.; Pizzi, G.; Kumagai, Y.; Oba, F.; Tanaka, I. Band structure diagram paths based on crystallography. *Comput. Mater. Sci.* **2017**, *128*, 140–184.

(52) Shannon, R. D. Revised effective ionic radii and systematic studies of interatomic distances in halides and chalcogenides. *Acta Crystallogr., Sect. A: Cryst. Phys., Diffraction, Theor. Gen. Crystallogr.* **1976**, *32*, 751–767.

(53) Kramida, A.; Ralchenko, Yu.; Reader, J.; NIST ASD Team. *NIST Atomic Spectra Database*, ver. 5.8; National Institute of Standards and Technology, Gaithersburg, MD, 2020. DOI: 10.18434/T4W30F (accessed 2021-10-19).

(54) Bekyarova, E.; Itkis, M. E.; Cabrera, N.; Zhao, B.; Yu, A.; Gao, J.; Haddon, R. C. Electronic properties of single-walled carbon nanotube networks. *J. Am. Chem. Soc.* **2005**, *127*, 5990–5995.

(55) Nirmalraj, P. N.; Lyons, P. E.; De, S.; Coleman, J. N.; Boland, J. J. Electrical connectivity in single-walled carbon nanotube networks. *Nano Lett.* **2009**, *9*, 3890–3895.

(56) Yu, L.; Shearer, C.; Shapter, J. Recent development of carbon nanotube transparent conductive films. *Chem. Rev.* **2016**, *116*, 13413–13453.

(57) Holland, P. L. Distinctive reaction pathways at base metals in high-spin organometallic catalysts. *Acc. Chem. Res.* **2015**, *48*, 1696–1702.

Recommended by ACS

Nanoscale Mapping of Carrier Mobilities in the Ballistic Transports of Carbon Nanotube Networks

Jeongsu Kim, Seunghun Hong, *et al.*

NOVEMBER 17, 2022
ACS NANO

READ 

Bridging the Junction: Electrical Conductivity of Carbon Nanotube Networks

Kevin Conley and Antti J. Karttunen

SEPTEMBER 30, 2022
THE JOURNAL OF PHYSICAL CHEMISTRY C

READ 

Complementary Transistors Based on Aligned Semiconducting Carbon Nanotube Arrays

Chenchen Liu, Zhiyong Zhang, *et al.*

NOVEMBER 23, 2022
ACS NANO

READ 

Designed Production of Atomic-Scale Nanowindows in Single-Walled Carbon Nanotubes

Yuki Nagata, Katsumi Kaneko, *et al.*

APRIL 13, 2023
LANGMUIR

READ 

Get More Suggestions >